Efficient Simulation of Quantum Error Correction Under Coherent Error Based on the Nonunitary Free-Fermionic Formalism

Yasunari Suzuki, Keisuke Fujii, and Masato Koashi

Efficient simulation of quantum error correction under coherent error based on non-unitary free-fermionic formalism

Yasunari Suzuki,[1, 2, *] Keisuke Fujii,[1, 2, 3, †] and Masato Koashi[1, 2, ‡]

[1] *Department of Applied Physics, Graduate School of Engineering,*
The University of Tokyo, 7-3-1 Hongo, Bunkyo-ku, Tokyo 113-8656, Japan
[2] *Photon Science Center, Graduate School of Engineering,*
The University of Tokyo, 7-3-1 Hongo, Bunkyo-ku, Tokyo 113-8656, Japan
[3] *JST, PRESTO, 4-1-8 Honcho, Kawaguchi, Saitama, 332-0012, Japan*

In order to realize fault-tolerant quantum computation, tight evaluation of error threshold under practical noise models is essential. While non-Clifford noise is ubiquitous in experiments, the error threshold under non-Clifford noise cannot be efficiently treated with known approaches. We construct an efficient scheme for estimating the error threshold of one-dimensional quantum repetition code under non-Clifford noise. To this end, we employ non-unitary free-fermionic formalism for efficient simulation of the one-dimensional repetition code under coherent noise. This allows us to evaluate the effect of coherence in noise on the error threshold without any approximation. The result shows that the error threshold becomes one third when noise is fully coherent. Our scheme is also applicable to the surface code undergoing a specific coherent noise model. The dependence of the error threshold on noise coherence can be explained with a leading-order analysis with respect to coherence terms in the noise map. We expect that this analysis is also valid for the surface code since it is a two-dimensional extension of the one-dimensional repetition code. Moreover, since the obtained threshold is accurate, our results can be used as a benchmark for approximation or heuristic schemes for non-Clifford noise.

Introduction.— Quantum error correction (QEC) is a key technology for building a scalable fault-tolerant quantum computer. According to the theory of fault-tolerant quantum computation, one can perform quantum computation with arbitrary accuracy if the error probability is below a certain threshold value [1–3]. The threshold values of various QEC schemes have been calculated under various assumptions of the noise models and degrees of rigor [4–21]. In the case of the noise model which only consists of probabilistic Clifford gates and Pauli measurement channels, such as depolarizing noise, the threshold value can be efficiently and accurately estimated numerically [6–9] by virtue of the Gottesman-Knill theorem [22, 23]. On the other hand, non-Clifford noise is unavoidable in practical experiments [24–26], but QEC circuits under non-Clifford noise cannot be treated with this approach. Specifically, it is theoretically predicted that coherent noise, which is non-Clifford and is caused, for example, by over rotation, can have negative effects on quantum error correction [27]. Therefore, massive effort has been made for evaluating the effect of noise coherence on the error threshold. Since the simulation of quantum circuits under arbitrary local noise sometimes becomes as hard as that of universal quantum computation, we cannot efficiently simulate QEC circuits under coherent noise with straightforward methods. While its computational cost can be relaxed in some extent [19–21], the tractable number of qubits with straightforward methods is limited. In the case of concatenated codes, there is an efficient method to analytically estimate the error threshold under non-Clifford noise [17]. However, this technique is not applicable to topological codes, which are more feasible in practical experiments [24–26, 28]. In

general, we may approximate non-Clifford noise by a Clifford channel for an efficient simulation [10–16], but the accuracy of the estimated threshold is sacrificed. An efficient and accurate scheme, which works for topological codes under non-Clifford noise, is still lacking.

Here, we construct an efficient and accurate scheme to simulate one-dimensional (1D) repetition code with repetitive parity measurements under coherent noise. While the 1D repetition code cannot protect a logical qubit from arbitrary single-qubit error, it is still able to capture a necessary ingredient for fault-tolerant QEC, and hence was experimentally demonstrated as a building block for scalable fault-tolerant quantum computation [24, 26]. The key idea in our scheme is reducing the QEC circuit of the 1D repetition code to a classically simulatable class of non-unitary free-fermionic dynamics, which is known as a variation of matchgate quantum computing [29–37]. As compared to the stochastic noise model, we find that the error threshold of the 1D repetition code becomes about one third when noise is fully coherent. The dependence of the error threshold on noise coherence is explained by using a leading-order analysis with respect to coherence terms of noise map. We expect that a similar analysis holds in the surface code [38–40], which is the most experimentally feasible QEC scheme, since the surface code is a two-dimensional extension of the 1D repetition code. Furthermore, our accurate results can be used as a benchmark for approximation or heuristic schemes for estimating the error threshold under non-Clifford noise.

Simulation of the 1D repetition code.— The quantum circuit of the 1D repetition code with repetitive parity measurements is shown in Fig. 1(a). In the 1D repeti-
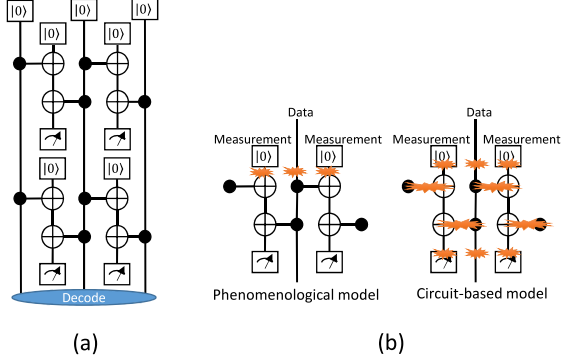
FIG. 1: (a) The QEC circuit of the 1D repetition code with $n = 3$. (b) The error allocation of the phenomenological (left) and circuit-based (right) models.

tion code, one logical bit a_{in} is encoded into physical n data qubits $\{|0\rangle^{\otimes n}, |1\rangle^{\otimes n}\}$, which are stabilized by operators $\{Z_i Z_{i+1}\}_{i=1}^{n-1}$, where $A_i (A \in \{X, Y, Z\})$ is the Pauli operator on the i-th data qubit. Error syndrome is measured through $(n-1)$ measurement qubits, each of which monitors the parities of the neighboring data qubits, i.e., $Z_i Z_{i+1}$. The measurements are repetitively performed for T cycles. The encoded bit is finally decoded from the data qubits and $T(n-1)$ syndromes, which can be efficiently done using minimum-weight perfect matching [24]. The probability with which the decoded bit a_{out} is flipped is defined as logical error probability p_{L}, which is the failure probability of the decoding.

Since the 1D repetition code is capable of correcting only X-type error, we consider a CPTP (completely positive trace-preserving) map of a general single-qubit X-type noise, which is regarded as a mixture of the X-type unitary (fully-coherent) and stochastic (incoherent) noise:

$$\mathcal{E}(\rho, X) = c e^{i\theta X} \rho e^{-i\theta X} + (1 - c)\left((1 - p)\rho + pX\rho X\right)$$
$$= \frac{1 + c}{2} e^{i\theta X} \rho e^{-i\theta X} + \frac{1 - c}{2} e^{-i\theta X} \rho e^{i\theta X}, \quad (1)$$

where θ is defined by $\cos\theta = \sqrt{1 - p}$ and $\sin\theta = \sqrt{p}$. The parameter c $(0 \le c \le 1)$, which we call noise coherence, is a measure of coherence in the noise. We call the parameter p $(0 \le p \le 1)$ as the physical error probability since it can be understood as the probability with which the input state $|0\rangle$ is measured as the output state $|1\rangle$. We consider two types of noise allocation models [41] as shown in Fig. 1(b). In the case of the phenomenological model, a noise map $\mathcal{E}(\rho, X)$ is located on each of the data and measurement qubits at the beginning of each cycle. In the case of the circuit-based model, the noise map is located at each time step of preparation, gate operation, and measurement, on every qubit including the one that is idle at the

time step. There, we assume that two-qubit noise map $p_{XI}\mathcal{E}(\rho, X \otimes I) + p_{IX}\mathcal{E}(\rho, I \otimes X) + p_{XX}\mathcal{E}(\rho, X \otimes X)$ acts on the output qubits after each controlled-Not (CNOT) operation. Since our noise models are symmetric over the bit values, we may choose $a_{\mathrm{in}} = 0$ to evaluate the logical error probability as $p_{\mathrm{L}} = \mathrm{Pr}(a_{\mathrm{out}} = 1)$.

Before reducing the noisy circuit to free-fermionic dynamics, we reformulate it as a sequence of generalized measurements on the data qubits, such that the state after each measurement is pure. We denote the outcome of the k-th measurement by t_k and the corresponding Kraus operator by $K_k^{(t_k)}$. The probability of a sequence of outcomes $\boldsymbol{t}_k := t_k...t_1$ is given by

$$\mathrm{Pr}(\boldsymbol{t}_k) = \Gamma(\boldsymbol{t}_k) := \langle 0^{\otimes n} | (\boldsymbol{K}^{(\boldsymbol{t}_k)})^\dagger \boldsymbol{K}^{(\boldsymbol{t}_k)} | 0^{\otimes n} \rangle, \quad (2)$$

where $\boldsymbol{K}^{(\boldsymbol{t}_k)} := K_k^{(t_k)} K_{k-1}^{(t_{k-1})} ... K_1^{(t_1)}$. We may identify three types of operations on data qubits to assign Kraus operators. For clarity, we describe the case of the phenomenological model. The first type is the single-qubit noise $\mathcal{E}$ given in Eq.(1). Its operation on the i-th qubits is equivalently described by Kraus operators $K_{\mathrm{noise},i}^{(\phi)} = \sqrt{p(\phi)} e^{i\phi X_i}$, where $\phi \in \{\pm\theta\}$ and $p(\pm\theta) := \frac{1 \pm c}{2}$. The second type is the parity measurement on the i-th and $(i + 1)$-th data qubits, which composed of a measurement qubit and two CNOT gates. Treating the noise map $\mathcal{E}$ on the measurement qubit as above, it can be represented by $K_{\mathrm{parity},i}^{(s,\phi)} = \sqrt{p(\phi)} \frac{1}{2}(I + (-1)^s e^{-2i\phi} Z_i Z_{i+1})$, where $s \in \{0, 1\}$ is the output of the parity measurement. In the case of the circuit-based model, we may still use the same form of $K_{\mathrm{parity},i}^{(s,\phi)}$ except for varying the probability mass function $p(\phi)$ (see Appendix A [42]). The third type appears in an alternate description of the decoding process. Though the input bit is usually decoded through noisy direct measurements of the data qubits and classical computation, we use the following equivalent process instead. We apply map $\mathcal{E}$ on each data qubit. We perform ideal parity measurements on neighboring data qubits, whose Kraus operator is given by $K_{\mathrm{parity},i}^{(s)} = \frac{1}{2}(I + (-1)^s Z_i Z_{i+1})$. Let k_f be the index of the last ideal parity measurement, and define $\boldsymbol{t} := \boldsymbol{t}_{k_f}$. Based on all the measured parities, which is included in $\boldsymbol{t}$, we choose a recovery operation $R(\boldsymbol{t}) = \prod_{i=1}^{n} X_i^{r_i(\boldsymbol{t})}$, where $r_i(\boldsymbol{t}) \in \{0, 1\}$ is determined using minimum-weight perfect matching [24, 43, 44]. The recovered state $R(\boldsymbol{t}) \boldsymbol{K}_{k_f}^{(\boldsymbol{t})} | 0\rangle^{\otimes n}$ is in the code space of the 1D repetition code, which should be written in the form $\alpha |0\rangle^{\otimes n} + \beta |1\rangle^{\otimes n}$. The decoded bit a_{out} is thus obtained by measuring the n-th qubit. The joint probability of obtaining $\boldsymbol{t}$ and a decoding failure is then given by

$$\mathrm{Pr}(a_{\mathrm{out}} = 1, \boldsymbol{t}) = \Gamma_{\mathrm{L}}(\boldsymbol{t})$$
$$:= \langle 0^{\otimes n} | (R(\boldsymbol{t}) \boldsymbol{K}^{(\boldsymbol{t})})^\dagger \frac{I - Z_n}{2} R(\boldsymbol{t}) \boldsymbol{K}^{(\boldsymbol{t})} | 0^{\otimes n} \rangle \quad (3)$$

From Eqs. (2) and (3), we have,

$$p_{\mathrm{L}} = \mathrm{Pr}(a_{\mathrm{out}} = 1) = \langle \Gamma_{\mathrm{L}}(\boldsymbol{t}) / \Gamma(\boldsymbol{t}) \rangle_{\boldsymbol{t}}, \quad (4)$$

which means that we can accurately calculate p_L by sampling $\boldsymbol{t}$ with probability $\Gamma(\boldsymbol{t})$ repeatedly and by taking the average of $\Gamma_L(\boldsymbol{t})/\Gamma(\boldsymbol{t})$. Since the sampling of $\boldsymbol{t}$ can be done by sequentially generating t_k according to $\Pr(t_k|\boldsymbol{t}_{k-1}) = \Gamma(\boldsymbol{t}_k)/\Gamma(\boldsymbol{t}_{k-1})$, the efficiency of this scheme follows that of computing $\Gamma(\boldsymbol{t}_k)$ and $\Gamma_L(\boldsymbol{t})$.

Reduction to non-unitary free-fermionic dynamics.— We use non-unitary free-fermionic dynamics to calculate $\Gamma(\boldsymbol{t}_k)$ and $\Gamma_L(\boldsymbol{t})$ efficiently. Let us briefly summarize the known facts about non-unitary free-fermionic dynamics [32, 37]. We define $\{c_i\}$ ($1 \leq i \leq 2n$) as the Majorana fermionic operators for n fermionic modes, which satisfy $\{c_i, c_j\} = 2\delta_{i,j}$, $c_i^\dagger = c_i$ and $c_i^2 = I$. The covariance matrix for a pure state $|\psi\rangle$ is defined as $M_{ij} = \frac{-i}{\langle\psi|\psi\rangle} \frac{\langle\psi|[c_i,c_j]|\psi\rangle}{2}$. We call the state $|\psi\rangle$ is a fermionic Gaussian state (FGS) iff the covariance matrix satisfies $MM^T = I$. An FGS can be fully specified by a pair (M, Γ), where Γ is the norm $\langle\psi|\psi\rangle$. The absolute value of the inner product of two FGSs, $|\psi\rangle \mapsto (M_\psi, \Gamma_\psi)$ and $|\phi\rangle \mapsto (M_\phi, \Gamma_\phi)$, is given by $|\langle\psi|\phi\rangle|^2 = 2^{-n}\Gamma_\psi\Gamma_\phi \det(M_\psi + M_\phi)$. An operator of form $e^{\sum_{i<j} \alpha_{ij} c_i c_j}$ with α_{ij} being a complex value is called a fermionic Gaussian operator (FGO). Note that FGOs are not necessarily unitary. An FGO maps any FGS to another FGS. Given an FGO G and an input FGS $|\psi\rangle \mapsto (M, \Gamma)$, the description (M', Γ') for the output state $G|\psi\rangle$ is calculated as follows. Consider a fermionic maximally entangled state $|\psi_M\rangle \mapsto (M_M, \Gamma_M)$ of $2n$ fermionic modes, which is defined by $M_M = \begin{pmatrix} 0 & I \\ -I & 0 \end{pmatrix}$ and $\Gamma_M = 1$. We calculate (M_G, Γ_G) corresponding to the state $|\psi_G\rangle = (G \otimes I)|\psi_M\rangle$. In terms of matrices A, B, D, which are defined by $\begin{pmatrix} A & B \\ -B^T & D \end{pmatrix} = M_G$, the output is calculated as $(M', \Gamma') = (A - B(M - D)^{-1}B^T, \Gamma_G\Gamma\sqrt{\det(M - D)})$. In this way, free-fermionic dynamics consisting of FGOs on FGSs can be simulated efficiently.

Now we are ready to reformulate the QEC process with non-unitary free-fermionic dynamics. Using the Jordan-Wigner transformation, we may choose $c_{2i-1} = \left(\prod_{j=1}^{i-1} X_j\right) Z_i$ and $c_{2i} = \left(\prod_{j=1}^{i-1} X_j\right) Y_i$. We see that $X_i = -ic_{2i}c_{2i-1}$ and $Z_iZ_{i+1} = -ic_{2i+1}c_{2i}$, which are both quadratic terms of the Majorana fermionic operators. Therefore, $K_{\text{noise},i}^{(\phi)}$, $K_{\text{parity},i}^{(s,\phi)}$, $K_{\text{parity},i}^{(s)}$ and R are FGOs. Unfortunately, the initial state $|0\rangle^{\otimes n}$ and the operator $\frac{I-Z_n}{2}$ for calculating $\Gamma_L(\boldsymbol{t})$ are not an FGS and an FGO, respectively. For an efficient simulation, we need a further trick as follows. (While similar tricks in Refs. [33, 35, 36] might be employed, the following construction is much simpler and more efficient for our purpose.) We add the $(n+1)$-th ancillary qubit and corresponding Majorana fermionic operators c_{2n+1}, c_{2n+2}. Using an FGS $|\tilde{\psi}\rangle := (|0\rangle^{\otimes(n+1)} + |1\rangle^{\otimes(n+1)})/\sqrt{2}$, it is not difficult

to show that

$$\Gamma(\boldsymbol{t}_k) = \langle\tilde{\psi}|(\boldsymbol{K}^{(\boldsymbol{t}_k)})^\dagger \boldsymbol{K}^{(\boldsymbol{t}_k)}|\tilde{\psi}\rangle, \tag{5}$$

$$\Gamma_L(\boldsymbol{t}) = \langle\tilde{\psi}|(R(\boldsymbol{t})\boldsymbol{K}^{(\boldsymbol{t})})^\dagger \frac{I - Z_n Z_{n+1}}{2} R(\boldsymbol{t})\boldsymbol{K}^{(\boldsymbol{t})}|\tilde{\psi}\rangle, \tag{6}$$

since $K^{(\boldsymbol{t}_k)}$ and $R(\boldsymbol{t})$ commute with $\prod_{j=1}^{n+1} X_j$. Hence, they can be efficiently calculated (see Appendix A [42] for detail).

Result.— We show the logical error probability p_L as a function of the physical error probability p under incoherent noise ($c = 0$) and fully coherent noise ($c = 1$) in Fig. 2. To observe clear behavior of the error threshold, we have varied the number T of cycles according to n as $T = n-1$. We also assumed uniform error probability for two-qubit noise, i.e. $p_{XI} = p_{IX} = p_{XX} = \frac{1}{3}$. We employed uniform weighting for performing minimum-weight perfect matching. The logical error probability p_L is expected to be exponentially small in the number of the data qubits n as far as the physical error probability p is below a certain value, which we call the error threshold p_{th}. By using the scaling ansatz [6, 9], we obtained the threshold values $p_{\text{th}} = 10.34(1)\%$ for $c = 0$ and $7.87(2)\%$ for $c = 1$ in the phenomenological model, and $3.243(6)\%$ for $c = 0$ and $1.040(5)\%$ for $c = 1$ in the circuit-based model. Our result for $c = 0$ in the case of the phenomenological model is consistent with the known results [6]. For more detailed procedures, see Appendix B [42]. We also confirmed exponential decay of logical error probability p_L with code distance d below the threshold value, which is approximated by $p_L \propto \left(\frac{p}{p_{\text{th}}}\right)^{d/2}$ regardless of the coherence of the noises (see Appendix E [42]).

Dependence of the error threshold p_{th} on the noise coherence c is shown in the insets of Fig. 2. We see that the error threshold p_{th} decreases as the noise coherence c increases. Note that non-uniform weighting improves the error threshold, but only slightly (see Appendix C [42]). The dependence on c can be explained with a leading-order analysis as follows. The noise map of Eq.(1) can be rewritten as $\mathcal{E}(\rho, X) = (1-p)\rho + ic\sqrt{(1-p)p}(X\rho - \rho X) + pX\rho X$. We call the second term $ic\sqrt{(1-p)p}(X\rho - \rho X)$ as the coherence term. This term contributes to diagonal terms of the density matrix only through a concatenation of multiple noise maps. The correction to the diagonal terms after several cycles is written as even-order terms in $c\sqrt{(1-p)p}$. For $p \ll 1$, the leading order of the correction is $O(p)$ in the circuit-based model, while it is $O(p^2)$ in the phenomenological model since an error on a data qubit spreads to two measurement qubits before the next noise map is applied on the data qubit. For example, the product of the coherence terms of noise maps located in the positions shown in Fig. 3 contributes the correction. In the case of the phenomenological model, the leading term is proportional to c^4p^2, and its sign depends on the results of previous syndrome measurements. Such a noise leads to space-time correlations in the syn-
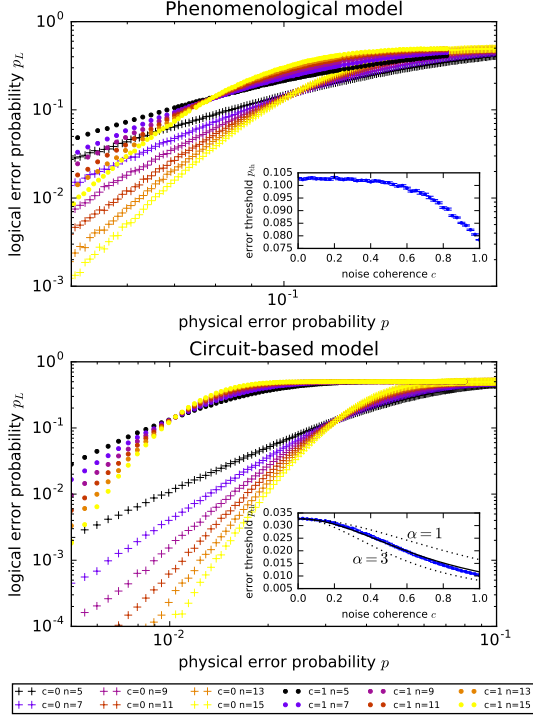
FIG. 2: The logical error probability p_{L} is plotted as a function of the physical error probability p for the two patterns of noise allocation. Insets show the error threshold p_{th} as a function of the amount of the coherence c. The blue dots are numerical results. The solid black curve in the circuit-based model is estimated behavior from the simulation of small-size QEC circuits. The dotted curves are drawn as references.
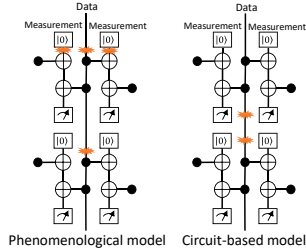

FIG. 3: The sets of coherent error allocations which contribute to the probability distribution of the syndrome measurements.

drome measurements. Since the decoder is not adapted to such correlations, the existence of coherence in noise is expected to result in a worse logical error probability. On the other hand, in the case of the circuit-based model, the leading term is proportional to $c^2 p$, and it always increases the error probability. This directly worsens the logical error probability and the error threshold.

In the case of the circuit-based model, we seek a

more quantitative explanation of the behavior by proposing a heuristic ansatz as follows. We define an effective physical error probability of a data qubit per cycle $p_{\mathrm{eff}}(p, c)$ (the precise definition is given in Appendix D [42]). The probability $p_{\mathrm{eff}}(p, c)$ should be expanded for small p as $p_{\mathrm{eff}}(p, c) = \beta(1 + \alpha c^2)p + O(p^2)$, where α is constant and is independent of the system size n. We assume that the logical error probability $p_{\mathrm{L}}(p, c)$ can be well explained by the local increase of noise, i.e., $p_{\mathrm{L}}(p, c) = p_{\mathrm{L}}((1 + \alpha c^2)p, 0)$. Based on this ansatz, the error threshold under coherent noise $p_{\mathrm{th}}(c)$ can be written as $p_{\mathrm{th}}(c) \sim \frac{p_{\mathrm{th}}(0)}{1 + \alpha c^2}$ if $p_{\mathrm{th}} \ll 1$. By using the analytically obtained value $\alpha = 11/6$ (see Appendix D [42]), this ansatz gives the solid curve in the inset of Fig. 2, which is in good agreement with the accurate numerical results. We may expect that a similar leading-order ansatz also holds for the surface code, since it is a two-dimensional extension of the 1D repetition code. The factor α is also easily obtained by analytically calculating the effective bit-flip probability, and $p_{\mathrm{th}}(0)$ for incoherent noises can be efficiently computed. Therefore, the error threshold of the surface code under coherent noise will be estimated by the same approach.

Conclusion and discussion.— We constructed an efficient and accurate scheme for estimating the error threshold of the 1D repetition code under coherent noise. We have calculated the error threshold under coherent noise in terms of the physical error probability p and the noise coherence c. The parameters p and c can be experimentally accessible by randomized and purity benchmarkings, respectively [45, 46]. We emphasize here that the proposed accurate and efficient scheme is not limited to the 1D repetition code. In fact, in Appendix F [42] we provide an example with a fully quantum code, which simulates the surface code under a phenomenological coherent noise model. We have also proposed a leading-order ansatz for the estimation of the error threshold under coherent noise, and found that it reproduces the accurate numerical results well. This suggests that the effect of the coherent noise on the surface code will be assessed by an analogous ansatz, which can be calculated easily. In more general terms, the obtained accurate error thresholds of the 1D repetition code will serve as a reference to test the accuracy of approximation or heuristic schemes for simulating non-Clifford noise, as was done for the leading-order ansatz.

* suzuki@qi.t.u-tokyo.ac.jp
† fujii@qi.t.u-tokyo.ac.jp
‡ koashi@qi.t.u-tokyo.ac.jp

[1] A. Y. Kitaev, Russian Mathematical Surveys **52**, 1191 (1997).
[2] E. Knill, R. Laflamme, and W. H. Zurek, in *Proceedings of the Royal Society of London A: Mathematical, Physical and Engineering Sciences*, Vol. 454 (The Royal Society, 1998) pp. 365–384.
[3] D. Aharonov and M. Ben-Or, in *Proceedings of the twenty-ninth annual ACM symposium on Theory of computing* (ACM, 1997) pp. 176–188.
[4] J. Fern, J. Kempe, S. Simic, and S. Sastry, in *IEEE Trans. on Automatic Control*, Vol. 51 (2006) pp. 448–459.
[5] D. Greenbaum and Z. Dutton, arXiv preprint arXiv:1612.03908 (2016).
[6] C. Wang, J. Harrington, and J. Preskill, Annals of Physics **303**, 31 (2003).
[7] D. S. Wang, A. G. Fowler, and L. C. L. Hollenberg, Physical Review A **83**, 020302 (2011).
[8] A. G. Fowler, A. C. Whiteside, and L. C. L. Hollenberg, Phys. Rev. Lett. **108**, 180501 (2012).
[9] A. M. Stephens, Physical Review A **89**, 022321 (2014).
[10] J. Ghosh, A. G. Fowler, and M. R. Geller, Physical Review A **86**, 062318 (2012).
[11] M. R. Geller and Z. Zhou, Physical Review A **88**, 012314 (2013).
[12] M. Gutiérrez, L. Svec, A. Vargo, and K. R. Brown, Physical Review A **87**, 030302 (2013).
[13] M. Gutiérrez and K. R. Brown, Physical Review A **91**, 022335 (2015).
[14] E. Magesan, D. Puzzuoli, C. E. Granade, and D. G. Cory, Physical Review A **87**, 012324 (2013).
[15] D. Puzzuoli, C. Granade, H. Haas, B. Criger, E. Magesan, and D. G. Cory, Physical Review A **89**, 022306 (2014).
[16] M. Gutiérrez, C. Smith, L. Lulushi, S. Janardan, and K. R. Brown, Physical Review A **94**, 042338 (2016).
[17] B. Rahn, A. C. Doherty, and H. Mabuchi, Physical Review A **66**, 032304 (2002).
[18] C. Chamberland, J. J. Wallman, S. Beale, and R. Laflamme, arXiv preprint arXiv:1612.02830 (2016).
[19] Y. Tomita and K. M. Svore, Physical Review A **90**, 062320 (2014).
[20] A. J. Ferris and D. Poulin, Phys. Rev. Lett. **113**, 030501 (2014).
[21] A. S. Darmawan and D. Poulin, arXiv preprint arXiv:1607.06460 (2016).
[22] D. Gottesman, arXiv preprint quant-ph/9807006 (1998).
[23] S. Aaronson and D. Gottesman, Physical Review A **70**, 052328 (2004).
[24] J. Kelly, R. Barends, A. Fowler, A. Megrant, E. Jeffrey, T. White, D. Sank, J. Mutus, B. Campbell, Y. Chen, *et al.*, Nature **519**, 66 (2015).
[25] A. Córcoles, E. Magesan, S. J. Srinivasan, A. W. Cross, M. Steffen, J. M. Gambetta, and J. M. Chow, Nature communications **6** (2015).
[26] D. Ristè, S. Poletto, M.-Z. Huang, A. Bruno, V. Vesterinen, O.-P. Saira, and L. DiCarlo, Nature communications **6** (2015).
[27] R. Kueng, D. M. Long, A. C. Doherty, and S. T. Flammia, Phys. Rev. Lett. **117**, 170502 (2016).
[28] D. A. Lidar and T. A. Brun, *Quantum error correction* (Cambridge University Press, 2013).
[29] L. G. Valiant, SIAM Journal on Computing **31**, 1229 (2002).
[30] B. M. Terhal and D. P. DiVincenzo, Physical Review A **65**, 032325 (2002).
[31] E. Knill, arXiv preprint quant-ph/0108033 (2001).
[32] S. Bravyi, in *Quantum Inf. and Comp.*, Vol. 5 (2005) pp. 216–238.
[33] S. Bravyi, arXiv preprint quant-ph/0507282 (2005).
[34] R. Jozsa and A. Miyake, in *Proceedings of the Royal Society of London A: Mathematical, Physical and Engineering Sciences*, Vol. 464 (The Royal Society, 2008) pp. 3089–3106.
[35] R. Jozsa, A. Miyake, and S. Strelchuk, in *Quantum Inf. and Comp.*, Vol. 15 (2015) pp. 541–556.
[36] D. J. Brod, Physical Review A **93**, 062332 (2016).
[37] S. Bravyi, M. Suchara, and A. Vargo, Physical Review A **90**, 032326 (2014).
[38] E. Dennis, A. Kitaev, A. Landahl, and J. Preskill, Journal of Mathematical Physics **43**, 4452 (2002).
[39] S. B. Bravyi and A. Y. Kitaev, arXiv preprint quant-ph/9811052 (1998).
[40] A. G. Fowler, M. Mariantoni, J. M. Martinis, and A. N. Cleland, Physical Review A **86**, 032324 (2012).
[41] A. J. Landahl, J. T. Anderson, and P. R. Rice, arXiv preprint arXiv:1108.5738 (2011).
[42] See supplemental material at ... for details of sampling scheme, fitting method of the error threshold, details of minimum-weight perfect matching, definition of the effective physical error probability, dropping rate of the logical error probability after the threshold, and the method how to simulate the surface coder under coherent errors efficiently, which includes Refs. [47, 48].
[43] J. Edmonds, Canadian Journal of mathematics **17**, 449 (1965).
[44] V. Kolmogorov, Mathematical Programming Computation **1**, 43 (2009).
[45] E. Knill, D. Leibfried, R. Reichle, J. Britton, R. B. Blakestad, J. D. Jost, C. Langer, R. Ozeri, S. Seidelin, and D. J. Wineland, Phys. Rev. A **77**, 012307 (2008).
[46] J. Wallman, C. Granade, R. Harper, and S. T. Flammia, New Journal of Physics **17**, 113020 (2015).
[47] N. C. Jones, R. Van Meter, A. G. Fowler, P. L. McMahon, J. Kim, T. D. Ladd, and Y. Yamamoto, Physical Review X **2**, 031007 (2012).
[48] R. Raussendorf, J. Harrington, and K. Goyal, New Journal of Physics **9**, 199 (2007).